Applied Catalysis B: Environmental 160–161 (2014) 658–665

Contents lists available at ScienceDirect

Applied Catalysis B: Environmental

journal homepage: www.elsevier.com/locate/apcatb

Enhanced photocatalytic performance of Ag_3PO_4 by simutaneous loading of Ag nanoparticles and Fe(III) cocatalyst

Huogen Yu [a,b,*], Guoqiang Cao [b], Feng Chen [b], Xuefei Wang [b,*], Jiaguo Yu [c], Ming Lei [d]

[a] State Key Laboratory of Silicate Materials for Architectures, Wuhan University of Technology, Wuhan 430070, People's Republic of China
[b] Department of Chemistry, School of Science, Wuhan University of Technology, Wuhan 430070, People's Republic of China
[c] State Key Laboratory of Advanced Technology for Material Synthesis and Processing, Wuhan University of Technology, Wuhan 430070, People's Republic of China
[d] School of Science, Beijing University of Posts and Telecommunications, Beijing 100876, People's Republic of China

ARTICLE INFO

Article history:
Received 28 March 2014
Received in revised form 7 June 2014
Accepted 11 June 2014
Available online 19 June 2014

Keywords:
Fe(III) cocatalyst
Plasmon resonance
Synergistic effect
Ag_3PO_4
Ag nanoparticle

ABSTRACT

Enhanced light absorption and effective separation of photogenerated charges are the main strategies to improve the photocatalytic performance of photocatalytic materials. In this study, the enhanced light absorption and effective separation of photogenerated charges in Ag_3PO_4 photocatalyst can be easily realized via the simultaneous loading of Ag nanoparticles and Fe(III) cocatalyst. In this case, the noble metallic Ag nanoparticles not only function as a visible-light active component to strongly absorb visible light owing to its localized surface plasmon resonance, but also can improve the bandgap visible-light absorption of Ag_3PO_4, resulting in the generation of more photogenerated charges. Photocatalytic experimental results suggested that the simultaneously modified Fe(III)/Ag–Ag_3PO_4 photocatalyst showed an obviously higher photocatalytic activity than the pure Ag_3PO_4, and single-component modified Fe(III)/Ag_3PO_4 and Ag–Ag_3PO_4 photocatalysts. On the basis of the experimental results, a possible synergistic effect mechanism of Ag nanoparticles and Fe(III) cocatalyst was proposed to account for the improved photocatalytic performance of Fe(III)/Ag–Ag_3PO_4 photocatalyst, namely, the metallic Ag nanoparticles cause an obviously enhanced visible-light absorption to produce more photogenerated charges, while the Fe(III) works as an effective active site for the following oxygen reduction to reduce the recombination rate of photogenerated electrons and holes. The present work can provide some new insight for the smart design and preparation of new high-performance photocatalytic materials.

1. Introduction

The improvement of photocatalytic efficiency is one of the most important goals in semiconductor photocatalysis for scientists because of its promising applications in environmental pollution and energy crisis [1–3]. It is well known that the main steps taking place during photocatalysis include: (i) production of photogenerated electrons and holes by photon absorption in semiconductor photocatalysts; (ii) transfer and separation of photogenerated charges; (iii) photocatalytic oxidization and reduction reactions on the photocatalyst surface [4]. Unfortunately, for the single-component photocatalysts such as TiO_2 and WO_3, the great majority of photo-generated electrons and holes recombine before involving the photocatalytic reactions, thus obtaining a low photocatalytic efficiency [5–8]. Early research demonstrates that noble metal cocatalysts (Pt, Au, Ag, Pd, etc.) can function as electron sinks to effectively promote the transfer of photogenerated electrons and thereby improve the photocatalytic efficiency [6,9–13]. However, the expensive cost of noble metals limits their widely practical applications. Therefore, it is highly desirable to develop low-cost and high-efficient cocatalysts to enhance photocatalytic efficiency of semiconductor photocatalysts. Recently, it is found that transition metal ions (Fe(III), Cu(II), Ni(II), etc.) can be used as cocatalysts to facilitate the improvement of photocatalytic activities for semiconductor photocatalysts [14–18]. For examples, our previous report found that after the modification of Cu(II) cocatalyst, the quantum efficiency of $Ti_{1-3x}W_xGa_{2x}O_2$ photocatalysts had a great increase from 0.093% to 13% for the gaseous decomposition of 2-propanol under visible light irradiation [19]. Additionally,

* Corresponding authors at: Department of Chemistry, School of Science, Wuhan University of Technology, Wuhan 430070, People's Republic of China.
Tel.: +86 27 87871029; fax: +86 27 87879468.
E-mail addresses: yuhuogen@whut.edu.cn (H. Yu), xuefei@whut.edu.cn (X. Wang).

http://dx.doi.org/10.1016/j.apcatb.2014.06.015
0926-3373/

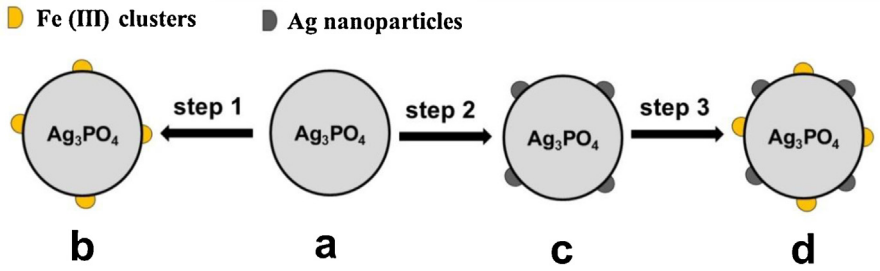

Fig. 1. Schematic diagram illustrating the controllable preparation of the various samples: (a) Ag_3PO_4; (b) Fe(III)/Ag_3PO_4; (c) Ag–Ag_3PO_4; and (d) Fe(III)/Ag–Ag_3PO_4. Steps 1 and 3: impregnation method; step 2: photoreduction method.

we also revealed that Fe(III)-cocatalyst modified TiO_2 photocatalyst exhibited an obviously higher photocatalytic activity with a QE value of 22% compared to N-doped TiO_2 (QE = 3.9%) [20]. Therefore, it is very interesting and important to develop transition metal cocatalyst-modified photocatalytic materials with high performance.

In addition to the effective separation of photogenerated charges by cocatalyst modification, the improved light absorption is another effective approach to improve the photocatalytic performance of semiconductor photocatalysts. It is well-known that noble metal nanoparticles (such as Au and Ag) can exhibit strong absorption in visible and even near-infrared regions by tuning their morphologies and compositions due to their localized surface plasmon resonance (LSPR) [21,22]. As a consequence, the noble metal nanoparticles have been widely investigated in photocatalytic field and are usually combined with semiconductor materials to improve their visible-light absorption efficiency. Especially, the noble metal nanoparticles can be loaded on the surface of wide bandgap semiconductors (such as TiO_2, ZrO_2 and AgCl) to develop visible-light photocatalyst by extending their light absorption range to visible-light region [23–25]. More importantly, the LSPR absorption of noble metal nanoparticles can also be used to further improve the visible-light absorption ability of narrow bandgap photocatalysts in addition to their original light absorption property [26,27]. After surface loading of noble metal nanoparticles, many investigations have demonstrated that the resulting noble metal-modified photocatalysts (or plasmonic photocatalysts) usually show an obviously enhanced visible-light photocatalytic performance [11,27,28]. However, from the view point of practical applications, it is highly required to develop new strategy to further improve the photocatalytic performance of the noble metal-modified photocatalysts.

In recent years, Ag_3PO_4 has been demonstrated to be an effective visible-light photocatalyst [29]. It is found that the previous investigations about the Ag_3PO_4 photocatalysts are mainly focused on the material nanonization, controlled morphology, and composite semiconductors, with the aim of improving its photocatalytic performance [30–33]. In this study, to further improve the photocatalytic performance of Ag_3PO_4, metallic Ag nanoparticles and Fe(III) cocatalyst are simultaneously loaded on its surface to prepare the highly efficient Fe(III)/Ag–Ag_3PO_4 visible-light photocatalyst. In this case, the noble metallic Ag nanoparticles not only work as a visible-light active component to strongly absorb visible light, but also improve the bandgap visible-light absorption of Ag_3PO_4 to produce more photogenerated charges, while the Fe(III) as an effective electron-transfer cocatalyst reduces the recombination of photogenerated electrons and holes via the rapid transfer of photogenerated electrons from the photocatalytic materials to oxygen. To the best of our knowledge, this is the first report about the enhanced photocatalytic performance of Ag_3PO_4 via simultaneous modification of noble metal nanoparticles and transition metal cocatalyst. This work may provide new insights for the design and fabrication of new high-efficiency visible-light photocatalysts.

2. Experimental

All the reagents were of analytical grade and were used without any further purification. Deionized water was used in all experiments.

2.1. Preparation of Ag_3PO_4 sample

The Ag_3PO_4 particles were prepared using a facile precipitation method. Briefly, 36 mL $AgNO_3$ aqueous solution (0.1 mol/L) and 16 mL Na_2HPO_4 (0.1 mol/L) were added to a 100 mL Teflon-lined stainless steel autoclave. Then the autoclave was kept in an electric oven at 60 °C for 2 h. After cooling down to room temperature, the yellow precipitate was collected by centrifugation and thoroughly washed with ethanol and distilled water for 3 times. The precipitate was finally dried at 60 °C overnight to obtain Ag_3PO_4 samples (Fig. 1a).

2.2. Preparation of Fe(III)/Ag_3PO_4 sample (Fe/Ag_3PO_4 = 0.1 wt%)

The Fe(III)/Ag_3PO_4 photocatalyst was prepared by an impregnation technique (Fig. 1b) [34]. In a typical preparation, 0.5 g of the as-prepared Ag_3PO_4 samples were dispersed into 10 mL $Fe(NO_3)_3$ solution (9 mmol/L) under stirring. After stirring for 15 min, the suspension solution was maintained at 60 °C for 2 h. The resultant powder was recovered by filtration, rinsed with distilled water, and dried at 60 °C to obtain the Fe(III)/Ag_3PO_4 photocatalyst. According to the investigation about the effect of Fe amount on the photocatalytic performance of Fe(III)/Ag_3PO_4, it was found that when the ratio of Fe to Ag_3PO_4 was 0.1 wt%, the resulting Fe(III)/Ag_3PO_4 photocatalyst showed the highest photocatalytic activity. Therefore, in this study, the amount of Fe(III) cocatalyst to Ag_3PO_4 was controlled to be 0.1 wt%, and the resulting sample was referred to as Fe(III)/Ag_3PO_4.

2.3. Preparation of Ag–Ag_3PO_4 sample (Ag/Ag_3PO_4 = 1 wt%)

The Ag–Ag_3PO_4 photocatalyst was prepared by a well-known photoreduction method (Fig. 1c) [11]. Briefly, 0.5 g of the as-prepared Ag_3PO_4 samples were dispersed into 9.26 mL $AgNO_3$ aqueous solution (5 mmol/L) to form a suspension solution, and 10 mL of methyl orange aqueous (20 mg/L) as the electron donor subsequently was added to the above solution. After vigorous stirring for 15 min at room temperature, the suspension solution was irradiated with a 350-W Xenon lamp (without filtering) for 30 min. The resulting samples were recovered by filtration, rinsed with purified water, and finally dried at 60 °C for 2 h. In this study, the

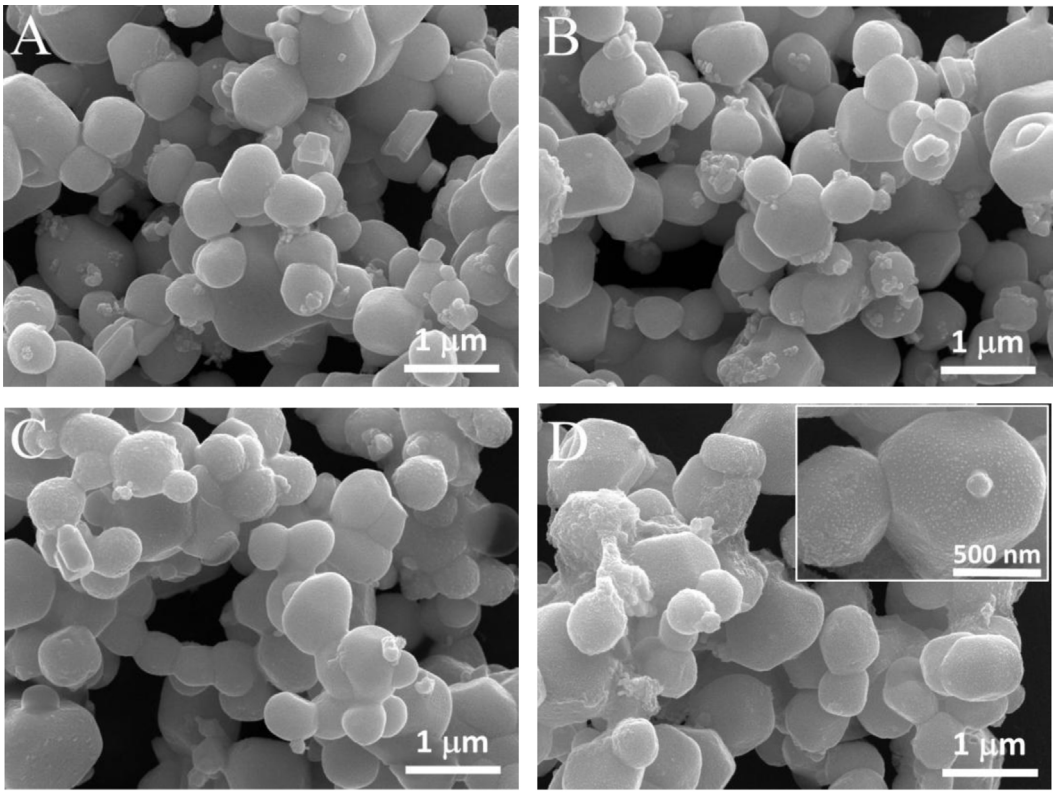

Fig. 2. FESEM images of the various samples: (A) Ag_3PO_4; (B) Fe(III)/Ag_3PO_4; (C) Ag–Ag_3PO_4; and (D) Fe(III)/Ag–Ag_3PO_4.

amount of metallic Ag to Ag_3PO_4 was controlled to be 1 wt%, and the resulting sample was referred to as Ag–Ag_3PO_4.

2.4. Preparation of Fe(III)/Ag–Ag_3PO_4 sample

The Fe(III)/Ag–Ag_3PO_4 photocatalyst (Fig. 1d) was prepared under an identical experimental condition as described in Section 2.2 by using the Ag–Ag_3PO_4 samples prepared in Section 2.3.

2.5. Characterization

Morphological analysis was performed by an S-4800 field-emission scanning electron microscope (FE-SEM, Hitachi, Japan) with an acceleration voltage of 10 kV. X-ray diffraction (XRD) patterns were obtained on a Rigaku Ultima III X-Ray Diffractometer (Japan) using Cu Kα radiation. UV–vis absorption spectra were obtained using a UV–visible spectrophotometer (UV-2550, SHIMADZU, Japan). X-ray photoelectron spectroscopy (XPS) measurements were done on a VG ESCALAB 210 XPS spectrometer system with Mg Kα source. All the binding energies were referenced to the C 1s peak at 284.8 eV of the surface adventitious carbon.

2.6. Photocatalytic activity

The visible-light photocatalytic activities of the prepared samples were evaluated by the photocatalytic decomposition of MO and phenol solutions at ambient temperature. Experimental details were shown as follows: 0.1 g of the sample was dispersed into 10 mL of MO solution (20 mg/L) or phenol solution (10 mg/L) in a disk with a diameter of ca. 5 cm. The solution was allowed to reach an adsorption–desorption equilibrium among the photocatalyst, organic substances, and water before irradiation. For the evaluation of visible-light photocatalytic activity, a 350 W xenon lamp equipped with a UV-cutoff filter (providing visible-light with ≥400 nm) was used as a visible-light source, and the average light intensity striking the surface of the reaction solution was about 40 mW cm^2. The concentration of MO (or phenol) was determined by an UV–visible spectrophotometer (UV-1240, SHIMADZU, Japan). After visible-light irradiation for some time, the reaction solution was centrifuged to measure the concentration of MO (or phenol). As for the MO (or phenol) aqueous solution with low concentration, its photocatalytic decolorization is a pseudo-first-order reaction and its kinetics may be expressed as $\ln(c/c_0) = -kt$, where k is the apparent rate constant, and c_0 and c are the MO (or phenol) concentrations at initial state and after irradiation for t min, respectively [35,36].

For the repeated photocatalytic performance, the photocatalysts were first separated by centrifugation, washed with distilled water, and were then redisperred into the MO (or phenol) solutions.

3. Results and discussion

3.1. Morphology and microstructures of Fe(III)/Ag–Ag_3PO_4

The preparation of various photocatalysts such as Ag_3PO_4, Fe(III)/Ag_3PO_4, Ag–Ag_3PO_4 and Fe(III)/Ag–Ag_3PO_4 can be easily controlled by a facile solution route, as shown in Fig. 1. Firstly, Ag_3PO_4 precursor particles were obtained via a precipitation reaction with a low temperature (60 °C). By a photoreduction method, the Ag–Ag_3PO_4 samples can then be prepared, while the Fe(III)/Ag_3PO_4 samples can be obtained by an impregnation method. Finally, the preparation of Fe(III)/Ag–Ag_3PO_4 samples is the simple combination of the above two methods.

The controlled preparation of above various Ag_3PO_4 samples can firstly be demonstrated by FESEM and XRD results. Fig. 2 shows the FESEM images of the Ag_3PO_4, Fe(III)/Ag_3PO_4, Ag–Ag_3PO_4 and Fe(III)/Ag–Ag_3PO_4. It can be seen that the pure Ag_3PO_4

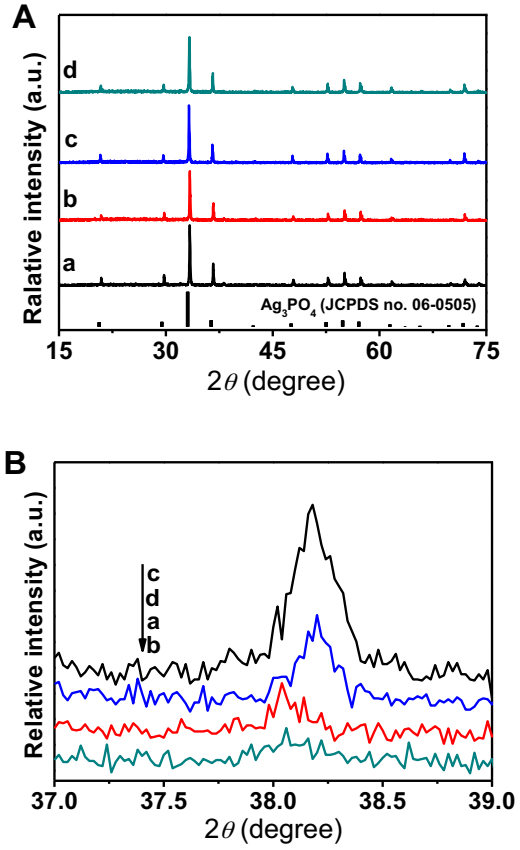

Fig. 3. (A) Wide-angle XRD patterns and (B) their corresponding diffraction peak of metallic Ag phase in various samples: (a) Ag_3PO_4; (b) Fe(III)/Ag_3PO_4; (c) Ag–Ag_3PO_4; and (d) Fe(III)/Ag–Ag_3PO_4.

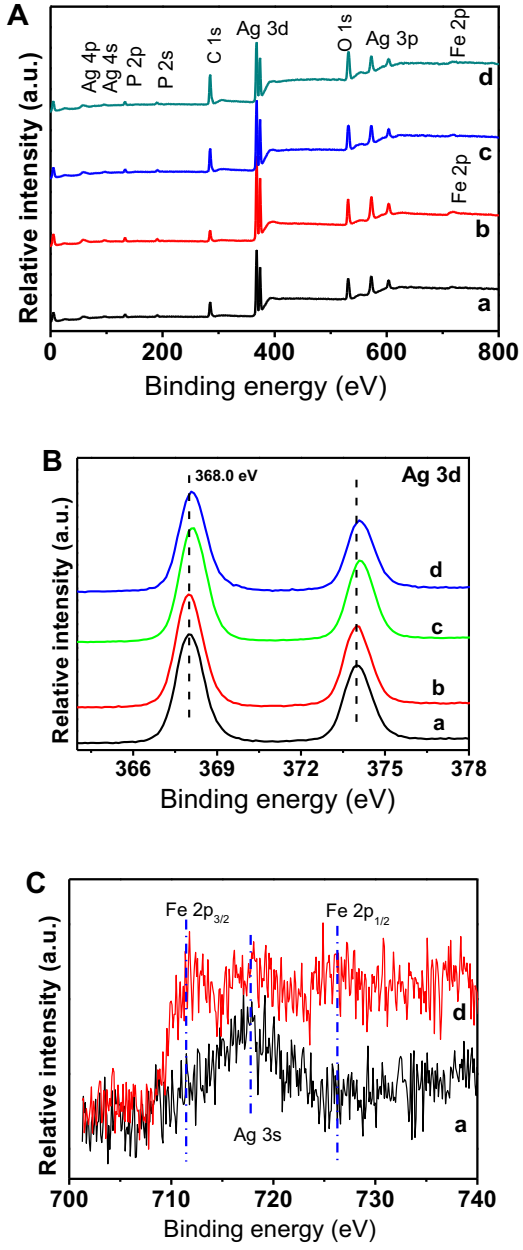

Fig. 4. XPS survey spectra (A), XPS spectra of Ag 3d (B) and Fe 2p (C) for the various samples: (a) Ag_3PO_4; (b) Fe(III)/Ag_3PO_4; (c) Ag–Ag_3PO_4; and (d) Fe(III)/Ag–Ag_3PO_4.

samples are composed of irregular particles with a size range from 0.2 to 1 μm and the particle surface is smooth (Fig. 2A). After their surface is modified with Fe(III) cocatalyst, the resulting Fe(III)/Ag_3PO_4 (Fig. 2B) shows a similar morphology as the Ag_3PO_4 sample due to a very low amount of Fe(III) cocatalyst (Fe(III)/Ag_3PO_4 = 0.1 wt%). As for the Ag–Ag_3PO_4 (Fig. 2C) and Fe(III)/Ag–Ag_3PO_4 (Fig. 2D) samples, they also show very similar particle morphologies with the pure Ag_3PO_4. However, further observation indicates that some small nanoparticles with a size of several nanometer can be observed (inset in Fig. 2D), which can be attributed to the Ag nanoparticles (see below XRD results). The crystal structures of different samples are further revealed by XRD patterns (Fig. 3A). It is clear that all the diffraction peaks of the Ag_3PO_4, Fe(III)/Ag_3PO_4, Ag–Ag_3PO_4 and Fe(III)/Ag–Ag_3PO_4 samples can be indexed to be the body-centered cubic structure of Ag_3PO_4 (JCPDS no. 06-0505) [29]. Moreover, all the samples show a comparable diffraction peak intensity and full width at half-maximum compared with the pure Ag_3PO_4 sample, suggesting that the crystallization and crystallite size of Ag_3PO_4 are not affected by the different modification processes owing to their mild conditions, in good agreement with the results observed in FESEM images. Considering the extremely small amount of metallic Ag on the Ag_3PO_4 surface, a carefully slow scan from 37° to 39° is employed to determine the diffraction peak of metallic Ag [36]. It is found that the Ag_3PO_4 and Fe(III)/Ag_3PO_4 samples show a very low intensity about the diffraction peak at ca. 38.1° (Fig. 3B), suggesting the formation of a very small amount of metallic Ag, which is mainly caused by the instability of intrinsic Ag_3PO_4 material. As for the Ag–Ag_3PO_4 and Fe(III)/Ag–Ag_3PO_4, an obviously enhanced diffraction peak of metallic Ag phase can be observed (Fig. 3B), indicating that the metallic Ag nanoparticles have been successfully loaded on the surface of Ag_3PO_4 by a photoreduction method, which can be clearly seen in FESEM image (inset in Fig. 2D). In addition, the carefully slow scan is also used to determine the diffraction peaks of possibly existing iron compounds (FeOOH, Fe_2O_3, etc.). However, no corresponding diffraction peaks in the Fe(III)-modified Ag_3PO_4 samples can be found (not shown here). According to our previous research, the possible reasons are that the amount of Fe(III) cocatalyst is extremely low and the Fe(III) cocatalyst with an amorphous form exists on the surface of Ag_3PO_4 as a result of the low-temperature synthesis [20].

XPS, an analytic technique about surface properties, is employed to further demonstrate the successful loading of metallic Ag and Fe(III) cocatalyst on the surface of Ag_3PO_4 sample. The XPS survey spectra of different samples are shown in Fig. 4A. It is clear that all the samples show the main binding energy peaks of Ag, P, and O

Table 1
Composition (atom %) of the various photocatalysts according to XPS analysis.

Samples	P	O	Ag	Fe
Ag_3PO_4	16.4	56.1	27.5	0
Fe(III)/Ag_3PO_4	12.6	66.3	18.3	2.8
Ag–Ag_3PO_4	14.4	61.1	24.5	0
Fe(III)/Ag–Ag_3PO_4	12.8	64.3	20.3	2.6

elements, which can be mainly ascribed to the Ag_3PO_4 and Ag phases, while the C element can be contributed to the adventitious hydrocarbon from XPS instrument itself. Compared with the pure Ag_3PO_4 and Ag–Ag_3PO_4 samples, new XPS peaks of Fe element are found in the Fe(III)/Ag_3PO_4 and Fe(III)/Ag–Ag_3PO_4 samples in addition to the Ag, P, O and C elements. The high-resolution XPS spectra further reveal the chemical states of Ag and Fe elements in Fig. 4B and C, respectively. For Ag_3PO_4 and Fe(III)/Ag_3PO_4, the binding energies of Ag $3d_{5/2}$ and Ag $3d_{3/2}$ are located at 368.0 and 374.0 eV, respectively, and the corresponding peaks are symmetric, which can mainly be attributed to the Ag^+ ions in Ag_3PO_4 (Fig. 3B) [37]. However, the peak positions of Ag $3d_{5/2}$ and Ag $3d_{3/2}$ obviously shift for Ag–Ag_3PO_4 and Fe(III)/Ag–Ag_3PO_4 compared to Ag_3PO_4 and Fe(III)/Ag_3PO_4, which indicates that metallic Ag^0 also exists in addition to the Ag^+ ions (Fig. 3B). Furthermore, it is clear that different from pure Ag_3PO_4, the Fe(III)/Ag–Ag_3PO_4 shows obvious peaks at ca. 711.5 eV (Fig. 3C), which corresponds to the binding energy of Fe $2p_{3/2}$ for the ferric ion [20,34]. According to the element component analysis based on the XPS results (Table 1), it is clear that the Fe(III) cocatalyst is about 2.6–2.8 at% on the surface of Fe(III)-modified Ag_3PO_4. These results indicate that metallic Ag and Fe(III) cocatalyst has successfully been loaded on the surface of Ag_3PO_4 photocatalyst.

Fig. 5 shows the UV–vis spectra of Ag_3PO_4, Fe(III)/Ag_3PO_4, Ag–Ag_3PO_4 and Fe(III)/Ag–Ag_3PO_4 samples. It is clear that the Fe(III)/Ag_3PO_4 shows a similar UV–vis spectrum as the pure Ag_3PO_4 owing to a very limited Fe(III) cocatalyst (Fig. 5a and b). After surface loading of metallic Ag nanoparticles, there is a slight increase in the whole absorption spectra, which can be caused by the LSPR of Ag nanoparticles [38,39]. In fact, the present UV–vis spectra of the samples are in good agreement with their colors (the inset of Fig. 5). However, it should be noted that in Ag_3PO_4 system, the LSPR of Ag nanoparticles is obviously lower than the well-known Ag/TiO_2 [11], Ag/AgBr [28], and Ag/AgCl [34] photocatalysts, in good agreement with the previous reports [40,41], which is possibly caused by their different dielectric environment of noble Ag nanoparticles.

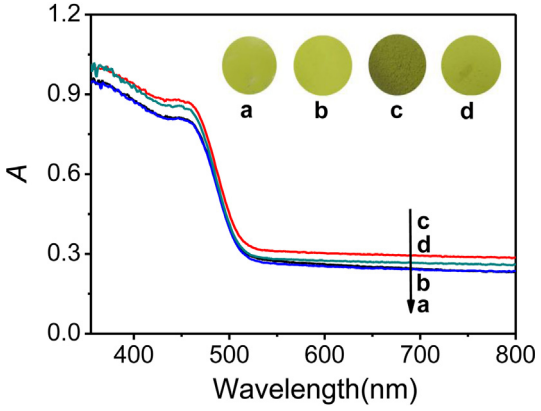

Fig. 5. UV–vis spectra of the various samples: (a) Ag_3PO_4; (b) Fe(III)/Ag_3PO_4; (c) Ag–Ag_3PO_4; and (d) Fe(III)/Ag–Ag_3PO_4. Inset showing their corresponding photographs.

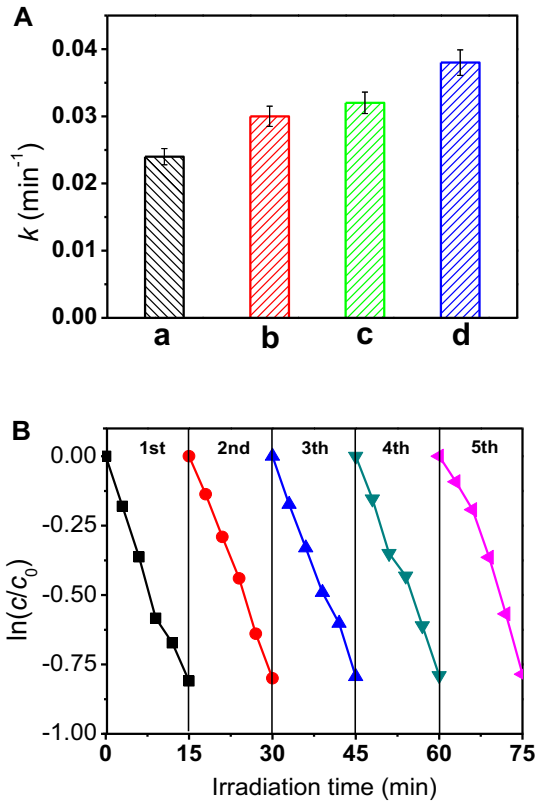

Fig. 6. (A) The rate constant (k) of the MO decomposition by various photocatalysts: (a) Ag_3PO_4; (b) Fe(III)/Ag_3PO_4; (c) Ag–Ag_3PO_4; and Fe(III)/Ag–Ag_3PO_4; (B) the repeated photocatalytic performance of Fe(III)/Ag–Ag_3PO_4 for the decomposition of phenol solution.

3.2. Photocatalytic performance and mechanism of Fe(III)/Ag–Ag_3PO_4

The photocatalytic performances of Ag_3PO_4, Fe(III)/Ag_3PO_4, Ag–Ag_3PO_4, and Fe(III)/Ag–Ag_3PO_4 samples were first evaluated by photocatalytic decolorization of MO aqueous solution under visible-light irradiation (Fig. S1). In the dark, no change in the concentration of MO was observed in the presence of different photocatalysts. Furthermore, visible-light illumination in the absence of photocatalysts did not result in the photocatalytic decolorization of MO. Fig. 6A shows the corresponding photocatalytic rate constant k of different photocatalysts. For Ag_3PO_4, it exhibits a relative high photocatalytic activity and the k value is about 0.024 min^{-1}. When the Fe(III) and metallic Ag are grafted on the Ag_3PO_4 surface, respectively, both of the resultant Fe(III)/Ag_3PO_4 and Ag–Ag_3PO_4 show an obviously improved photocatalytic performance with a k value of 0.03 and 0.032 min^{-1}. More specifically, the Fe(III)/Ag–Ag_3PO_4 photocatalyst possesses the highest photocatalytic activity for the discoloration rate of MO (k = 0.038 min^{-1}). To further investigate the performance stability of the Fe(III)/Ag–Ag_3PO_4 photocatalyst, five cycles were carried out for the photocatalytic decomposition of phenol solution, and the corresponding results are shown in Fig. 6B. It is found that the Fe(III)/Ag–Ag_3PO_4 photocatalyst can maintain a stable and efficient photocatalytic performance.

It is very interesting and meaningful to investigate the potential photocatalytic mechanism of Fe(III)/Ag–Ag_3PO_4 photocatalyst. It is clear that the Ag_3PO_4 photocatalyst exhibits strong oxidation ability for the photocatalytic decomposition of organic pollution such as MO and phenol (Fig. 7a). However, it possesses relatively weak reduction ability due to the higher potential of

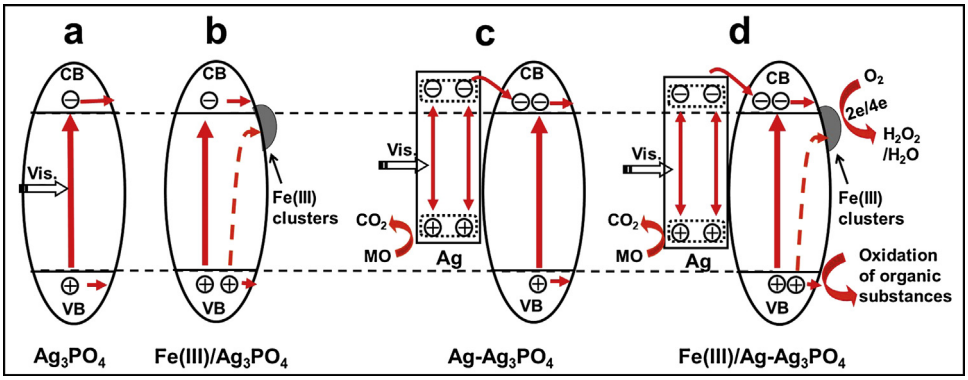

Fig. 7. Schematic diagrams illustrating the possible photocatalytic mechanism of various photocatalysts: (a) Ag_3PO_4; (b) Fe(III)/Ag_3PO_4; (c) Ag–Ag_3PO_4; and Fe(III)/Ag–Ag_3PO_4.

its conduction band (+0.45 V vs. SHE) compared with O_2/HO_2 (−0.046 V, vs. SHE) [42], which means that it is difficult to transfer photo-generated electrons by the way of one-electron transfer. However, the photocatalytic experimental result indicates that the photogenerated electrons on the Ag_3PO_4 CB can be successfully transferred, resulting in an effective decomposition of organic substances (Fig. 6). Thus, it is possible that multi-electron transfer of oxygen reduction (such as $O_2 + 2e^- + 2H^+ = H_2O_2$(aq), +0.682 V vs. SHE; $O_2 + 4e^- + 4H^+ = 2H_2O$(aq), +1.23 V vs. SHE) takes place on the active sites of the Ag_3PO_4 surface (Fig. 7a) [43]. As multi-electron transfer is a more complicated and difficult route compared with one-electron transfer, the Ag_3PO_4 photocatalyst exhibits a relative low photocatalytic activity (Fig. 6). When the Fe(III) ions are grafted onto the surface of Ag_3PO_4 to form Fe(III)/Ag_3PO_4 photocatalyst, the photogenerated electrons on the Ag_3PO_4 CB can easily transfer to the Fe(III) cocatalyst owing to its more positive potential of Fe^{3+}/Fe^{2+} (0.771 V, vs. SHE) [43] than the CB of Ag_3PO_4 (+0.45 V, vs. SHE), which promoting the rapid separation of photo-generated electrons and holes, and resulting in an enhanced photocatalytic performance (Fig. 7b). In fact, the Fe(III) as an effective multi-electron transfer cocatalyst for the oxygen reduction has been reported in TiO_2 and AgBr photocatalysts to increase the photocatalytic efficiency in our previous studies [20,34]. It is clear that the Fe(III) cocatalyst can accept a photogenerated electron to form Fe(II), which is unstable and easily becomes Fe(III) through the multi-electron reduction of oxygen under ambient conditions ($4Fe^{2+} + O_2 + 4H^+ \rightarrow 4Fe^{3+} + 2H_2O$ or $4Fe^{2+} + O_2 + 2H_2O \rightarrow 4Fe^{3+} + 2OH^-$), namely, the Fe(III) can be well recovered via the effective oxidation of Fe(II) by oxygen. A similar multi-electron oxygen reduction was also found on the Cu(II), Ag_2O and Pt cocatalysts [19,35,44]. Owing to the rapid capture of photogenerated electrons by Fe(III) cocatalyst, the recombination rate of photogenerated charges in the bulk and surface of Ag_3PO_4 photocatalysts can be significantly decreased, leading to an improvement of photocatalytic performance of Fe(III)/Ag_3PO_4. Compared with the Fe(III)/Ag_3PO_4 photocatalyst, the Ag/Ag_3PO_4 shows an obviously different enhanced mechanism (Fig. 7c). Under visible-light irradiation, Ag nanoparticles can produce photo-generated electrons and holes due to their LSPR absorption in addition to the intrinsic bang-gap excitation of Ag_3PO_4. The produced electrons can effectively transfer to the CB of Ag_3PO_4, while the photogenerated holes stay on the Ag nanoparticles to decompose organic substances. In addition, according to the UV–vis spectra (Fig. 5), it is clear that the bang-gap absorption of Ag_3PO_4 in the visible-light range of 400–500 nm is improved by the surface loading of metallic Ag nanoparticles. As many researchers have demonstrated that the produced rate of photogenerated electrons and holes in a semiconductor is proportional to the local electric-field intensity [26,45], the enhanced local electric field by Ag nanoparticles would facilitate the generation of more charges in Ag_3PO_4 phase. Therefore, it is clear that the formation of more photogenerated electrons and holes in Ag/Ag_3PO_4 contributes to its improved photocatalytic performance.

When both of the Fe(III) cocatalyst and Ag nanoparticles are simultaneously deposited on the surface of Ag_3PO_4, it is clearly found that the photocatalytic performance of resulting Fe(III)/Ag–Ag_3PO_4 photocatalyst can be further improved, which can be well explained by the synergistic effect of Fe(III) and Ag nanoparticles. The loading of Ag nanoparticles leads to the production of more photogenerated charges in Fe(III)/Ag–Ag_3PO_4 via LSPR absorption of Ag nanoparticles and enhanced band-gap absorption of Ag_3PO_4, while the Fe(III) cocatalyst provides as an active site for oxygen reduction reaction by effective transfer of photogenerated electrons to oxygen. In other words, the Fe(III)/Ag–Ag_3PO_4 photocatalyst integrates the advantages of Fe(III)/Ag_3PO_4 and Ag–Ag_3PO_4, and thus exhibits the highest photocatalytic performance.

3.3. *The synergistic effect of Fe(III) and metallic Ag cocatalyst*

To further demonstrate the synergistic effect of Fe(III) and metallic Ag cocatalyst for the enhanced photocatalytic performance of Fe(III)/Ag–Ag_3PO_4, a series of controlled experiments are performed (Fig. 8). Firstly, metallic Ag nanoparticles on the surface of Fe(III)/Ag–Ag_3PO_4 photocatalyst are selectively removed by H_2O_2. As the redox potential of H_2O_2/H_2O (+1.763 V vs. SHE) [43] is obviously higher than that of Ag^+/Ag (+0.7991 V vs. SHE), the metallic Ag can be effectively oxidized to Ag^+ ions, which can be clearly demonstrated by its colour change from the grayish yellow to completely yellow (Fig. 8B-a and b). In this case, the corresponding k value of the resultant sample decreases from 0.038 to 0.029 min^{-1}, a value comparable to that of the Fe(III)/Ag_3PO_4 photocatalyst (Fig. 6A). In addition, when the Fe(III)/Ag–Ag_3PO_4 sample is treated in a H_3PO_4 aqueous solution (pH 2), it is found that no Fe element can be found in the EDX result compared with the as-prepared sample (Fig. 9B and C), while the resulting sample still shows a greyish yellow colour (Fig. 8B-c) and a similar particle size of Ag_3PO_4 with Ag nanoparticles on its surface (Fig. 9A). Therefore, the above results strongly demonstrate the successfully selective removal of Fe(III) cocatalyst from Fe(III)/Ag–Ag_3PO_4 surface after H_3PO_4 treatment. The corresponding photocatalytic results suggest that there is a slight decrease about the rate constant (k = 0.031 min^{-1}) (Fig. 8C-c). With further selective removal of Ag nanoparticles by H_2O_2, the resulting sample shows a further decreased performance (k = 0.023 min^{-1}) (Fig. 8C-d) and it colour changes into yellow completely (Fig. 8B-d). Therefore, the above controlled experimental results strongly support that the synergistic effect of Fe(III) and

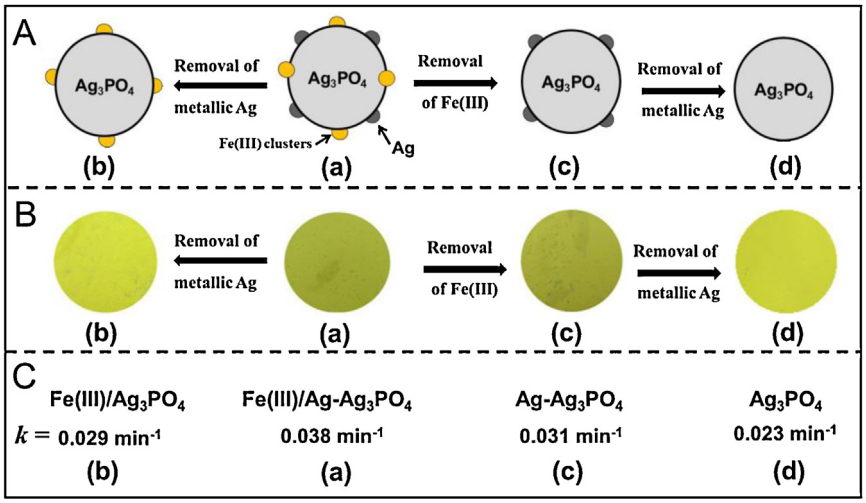

Fig. 8. (A) Schematic diagrams illustrating the selective removal of metallic Ag and Fe(III) cocatalyst from the Fe(III)/Ag–Ag_3PO_4 surface; (B) the corresponding photographs and (C) rate constant (k) of the resultant various samples: (a) Fe(III)/Ag–Ag_3PO_4; (b) Fe(III)/Ag_3PO_4 obtained from sample (a) after removal of metallic Ag; (c) Ag–Ag_3PO_4 obtained from sample (a) after removal of Fe(III); and (d) Ag_3PO_4 obtained from sample (a) after removal of Ag and Fe(III) cocatalyst.

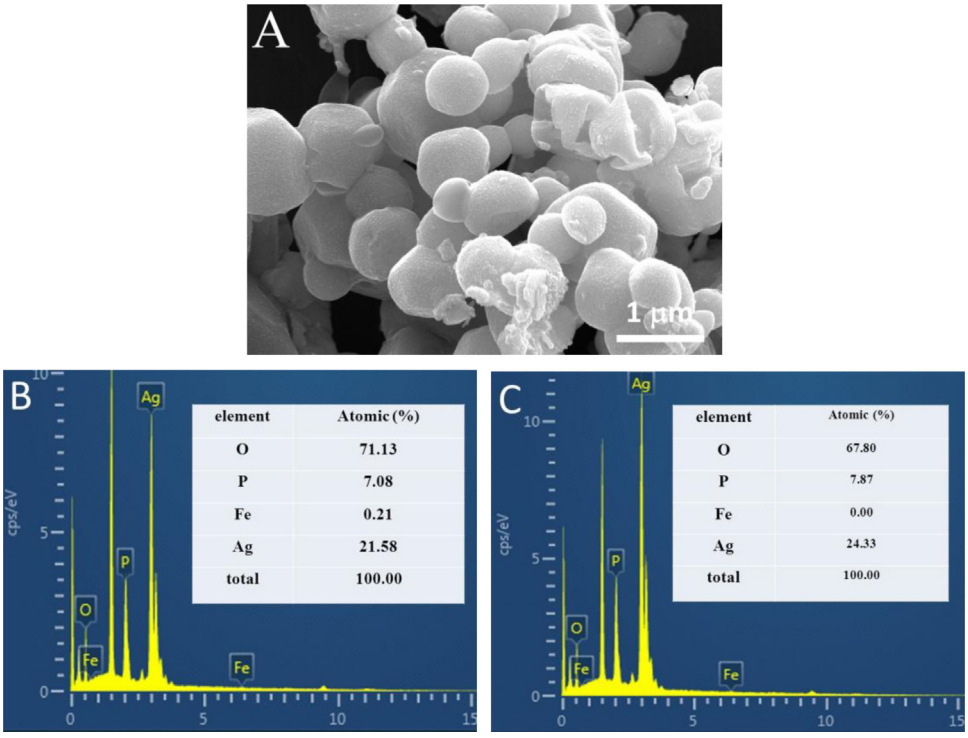

Fig. 9. FESEM image of the Fe(III)/Ag–Ag_3PO_4 after removal of Fe(III) cocatalyst by H_3PO_4; EDX spectra of the Fe(III)/Ag–Ag_3PO_4 before (B) and after (c) removal of Fe(III) cocatalyst by H_3PO_4.

metallic Ag cocatalysts is the main factor for the enhanced photocatalytic activity of Fe(III)/Ag–Ag_3PO_4, namely, the addition of metallic Ag nanoparticles causes an obviously enhanced visible-light absorption in photocatalyst to produce more photogenerated charges, while the Fe(III) works as an effective active site for the following oxygen reduction to reduce the recombination rate of photogenerated electrons and holes.

4. Conclusions

In summary, metallic Ag nanoparticles and Fe(III) cocatalysts were simultaneously loaded on the surface of Ag_3PO_4 to prepare the highly efficient Fe(III)/Ag–Ag_3PO_4 photocatalyst by a simple photoreduction-impregnation method. It was found that the metallic Ag nanoparticles not only function as a visible-light active component to strongly absorb visible light owing to its LSPR, but also can improve the bandgap visible-light absorption of Ag_3PO_4 due to the enhanced local electric field by Ag nanoparticles, resulting in the generation of more photogenerated charges. Compared with the pure Ag_3PO_4, Ag–Ag_3PO_4, and Fe(III)/Ag_3PO_4, the photocatalytic performance of Ag_3PO_4 photocatalyst could be greatly improved by the surface loading of Ag nanoparticles and Fe(III) cocatalyst. On the basis of the experimental results, an possible synergistic effect mechanism of Ag nanoparticles and Fe(III) cocatalyst was proposed to account for the improved photocatalytic performance of Fe(III)/Ag–Ag_3PO_4 photocatalyst, namely, the metallic Ag

nanoparticles cause an obviously enhanced visible-light absorption to produce more photogenerated charges, while the Fe(III) works as an effective active site for the following oxygen reduction to reduce the recombination rate of photogenerated electrons and holes. The present work can provide some new insight for the smart design and preparation of new high-performance photocatalytic materials.

Acknowledgements

This work was partially supported by the National Natural Science Foundation of China (21277107 and 51208396), the program for new century excellent talents in university (NCET-13-0944), and 973 Program (2013CB632402). This work was also financially supported by Wuhan Youth Chenguang Program of Science and Technology (2014070404010207) and Fundamental Research Funds for the Central Universities (Grant 2013-1a-036, 2013-1a-039). We thank FGM group at Wuhan University of Technology for assistance with XRD and SEM measurements.

Appendix A. Supplementary data

Supplementary data associated with this article can be found, in the online version, at http://dx.doi.org/10.1016/j.apcatb.2014.06.015.

References

[1] S.G. Kumar, L.G. Devi, Journal of Physical Chemistry A 115 (2011) 13211–13241.
[2] Q.J. Xiang, J.G. Yu, M. Jaroniec, Chemical Society Reviews 41 (2012) 782–796.
[3] M.C. Long, Y.L. Qin, C. Chen, X.Y. Guo, B.H. Tan, W.M. Cai, Journal of Physical Chemistry C 117 (2013) 16734–16741.
[4] A. Fujishima, X.T. Zhang, D.A. Tryk, Surface Science Reports 63 (2008) 515–582.
[5] T. Kamegawa, R. Kido, D. Yamahana, H. Yamashita, Microporous and Mesoporous Materials 165 (2013) 142–147.
[6] H. Tada, T. Kiyonaga, S. Naya, Chemical Society Reviews 38 (2009) 1849–1858.
[7] P. Wang, J. Wang, X.F. Wang, H.G. Yu, J.G. Yu, M. Lei, Y.G. Wang, Applied Catalysis B: Environmental 132 (2013) 452–459.
[8] Z.G. Zhao, Z.F. Liu, M. Miyauchi, Chemical Communications 46 (2010) 3321–3323.
[9] P. Li, Z. Wei, T. Wu, Q. Peng, Y.D. Li, Journal of the American Chemical Society 133 (2011) 5660–5663.
[10] G.C. Xi, J.H. Ye, Q. Ma, N. Su, H. Bai, C. Wang, Journal of the American Chemical Society 134 (2012) 6508–6511.
[11] R. Liu, P. Wang, X.F. Wang, H.G. Yu, J.G. Yu, Journal of Physical Chemistry C 116 (2012) 17721–17728.
[12] J. Du, J. Qi, D. Wang, Z.Y. Tang, Energy & Environmental Science 5 (2012) 6914–6918.
[13] K. Fuku, T. Kamegawa, K. Mori, H. Yamashita, Chemistry: An Asian Journal 7 (2012) 1366–1371.
[14] H. Irie, S. Miura, K. Kamiya, K. Hashimoto, Chemical Physics Letters 457 (2008) 202–205.
[15] M. Liu, X.Q. Qiu, M. Miyauchi, K. Hashimoto, Chemistry of Materials 23 (2011) 5282–5286.
[16] X.Q. Qiu, M. Miyauchi, H.G. Yu, H. Irie, K. Hashimoto, Journal of the American Chemical Society 132 (2010) 15259–15267.
[17] H. Irie, T. Shibanuma, K. Kamiya, S. Miura, T. Yokoyama, K. Hashimoto, Applied Catalysis B: Environmental 96 (2010) 142–147.
[18] X.Q. Qiu, M. Miyauchi, K. Sunada, M. Minoshima, M. Liu, Y. Lu, D. Li, Y. Shimodaira, Y. Hosogi, Y. Kuroda, K. Hashimoto, ACS Nano 6 (2012) 1609–1618.
[19] H. Yu, H. Irie, K. Hashimoto, Journal of the American Chemical Society 132 (2010) 6898–6899.
[20] H. Yu, H. Irie, Y. Shimodaira, Y. Hosogi, Y. Kuroda, M. Miyauchi, K. Hashimoto, Journal of Physical Chemistry C 114 (2010) 16481–16487.
[21] M.S. Wang, C.B. Gao, L. He, Q.P. Lu, J.Z. Zhang, C. Tang, S. Zorba, Y.D. Yin, Journal of the American Chemical Society 135 (2013) 15302–15305.
[22] C.H. An, S.N. Peng, Y.G. Sun, Advanced Materials 22 (2010) 2570–2574.
[23] K. Awazu, M. Fujimaki, C. Rockstuhl, J. Tominaga, H. Murakami, Y. Ohki, N. Yoshida, T. Watanabe, Journal of the American Chemical Society 130 (2008) 1676–1680.
[24] X. Chen, H.Y. Zhu, J.C. Zhao, Z.T. Zheng, X.P. Gao, Angewandte Chemie-International Edition 47 (2008) 5353–5356.
[25] X.F. Wang, S.F. Li, H.G. Yu, J.G. Yu, Journal of Molecular Catalysis A: Chemical 334 (2011) 52–59.
[26] X.M. Zhang, Y.L. Chen, R.S. Liu, D.P. Tsai, Reports on Progress in Physics 76 (2013) 046401.
[27] D.B. Ingram, S. Linic, Journal of the American Chemical Society 133 (2011) 5202–5205.
[28] P. Wang, T.S. Ming, G.H. Wang, X.F. Wang, H.G. Yu, J.G. Yu, Journal of Molecular Catalysis A: Chemical 381 (2014) 114–119.
[29] Z.G. Yi, J.H. Ye, N. Kikugawa, T. Kako, S.X. Ouyang, H. Stuart-Williams, H. Yang, J.Y. Cao, W.J. Luo, Z.S. Li, Y. Liu, R.L. Withers, Nature Materials 9 (2010) 559–564.
[30] Y.P. Bi, H.Y. Hu, S.X. Ouyang, G.X. Lu, J.Y. Cao, J.H. Ye, Chemical Communications 48 (2012) 3748–3750.
[31] Y.P. Bi, S.X. Ouyang, J.Y. Cao, J.H. Ye, Physical Chemistry Chemical Physics 13 (2011) 10071–10075.
[32] J. Guo, S. Ouyang, P. Li, Y. Zhang, T. Kako, J. Ye, Applied Catalysis B: Environmental 134–135 (2013) 286–292.
[33] Y.P. Liu, L. Fang, H.D. Lu, Y.W. Li, C.Z. Hu, H.G. Yu, Applied Catalysis B: Environmental 115 (2012) 245–252.
[34] H.G. Yu, L.L. Xu, P. Wang, X.F. Wang, J.G. Yu, Applied Catalysis B: Environmental 144 (2014) 75–82.
[35] H.G. Yu, R. Liu, X.F. Wang, P. Wang, J.G. Yu, Applied Catalysis B: Environmental 111 (2012) 326–333.
[36] X.F. Wang, S.F. Li, H.G. Yu, J.G. Yu, S.W. Liu, Chemistry – A European Journal 17 (2011) 7777–7780.
[37] H. He, Y. Li, X. Zhang, Y. Yu, C. Zhang, Applied Catalysis A – General 375 (2010) 258–264.
[38] G.Q. Luo, X.J. Jiang, M.J. Li, Q. Shen, L.M. Zhang, H.G. Yu, ACS Applied Materials & Interfaces 5 (2013) 2161–2168.
[39] C.S. Warren, E. Thimsen, Energy & Environmental Science 5 (2012) 5133–5146.
[40] Y. Hou, F. Zuo, Q. Ma, C. Wang, L. Bartels, P.Y. Feng, Journal of Physical Chemistry C 116 (2012) 20132–20139.
[41] P.Y. Dong, Y.H. Wang, B.C. Cao, S.Y. Xin, L.N. Guo, J. Zhang, F.H. Li, Applied Catalysis B: Environmental 132–133 (2013) 45–53.
[42] W.G. Wang, B. Cheng, J.G. Yu, G. Liu, W.H. Fan, Chemistry – An Asian Journal 7 (2012) 1902–1908.
[43] A.J. Bard, R. Parsons, J. Jordan, Standard Potentials in Aqueous Solution, Marcel Dekker, New York, 1985.
[44] R. Abe, H. Takami, N. Murakami, B. Ohtani, Journal of the American Chemical Society 130 (2008) 7780–7781.
[45] J. Lee, T. Javed, T. Skeini, A.O. Govorov, G.W. Bryant, N.A. Kotov, Angewandte Chemie-International Edition 45 (2006) 4819–4823.